Wall and Divertor Load during ELMy H-mode and Disruptions in ASDEX Upgrade

A. Herrmann, J. Neuhauser, G. Pautasso, V. Bobkov, R. Dux, T. Eich, C.J. Fuchs, O. Gruber, C. Maggi, H.W. Müller, V. Rohde, M. Y. Ye, ASDEX Upgrade team

Max-Planck-Institut für Plasmaphysik, EURATOM-IPP Association, Garching, Germany

e-mail contact of main author: albrecht.herrmann@ipp.mpg.de

Abstract: Measurements at the divertor tokamak ASDEX Upgrade reveal that non-divertor components receive up to 10% of the heating energy during plasma discharges. Infrared cameras were used to characterize heat deposition to the upper and lower divertor, and to all other significant in-vessel components, such as the central column, the ICRH and the protection limiters. The time and space resolution allow resolving ELM structures. In addition, the bolometry evaluation algorithm was improved to get power balances during ELMs. Whereas the non-divertor load is no problem in ASDEX Upgrade it might cause serious problems for experiments with large volume and energy content. This paper will present results on three selected topics with emphasis on ITER significance. (i) heat load and power decay length remote from the separatrix as well as ELM power balance (ii) ELM structures, and (iii) heat load pattern during disruptions.

1. Introduction

Plasma events, such as edge localized modes (ELMs) and disruptions eject significant amounts of plasma energy on short time-scales into the scrape-off layer (SOL) and finally to the divertor and main chamber walls. Whereas the absolute amount of energy released during such events is no real concern in present machines with carbon as first wall material, it might be intolerable in a next step device, such as ITER, because the plasma energy will increase like $\sim R^{\gamma}$, with $\gamma > 3$, due to the elementary scaling of the plasma energy, $W \sim \beta_t B_t^2 R^3$, and the fact that existing devices have either substantially smaller B_t than ITER and/or do not have the heating power to approach the critical β_t at full field [1]. This means, that the plasma energy increases stronger with major radius, R, than the available area for heat removal. Present scalings of the divertor heat flux profile width to ITER show no significant broadening but rather a weak steepening [2, 3], so that the wetted area in the divertor rises at most linearly with R. The inner vessel surface increases as R^2. The fraction of plasma stored energy, ejected by ELMs and disruptions, in ITER will be comparable to or higher than in present experiments [2]. From this it is expected for ITER that the heat flux to the divertor and the inner wall becomes significantly higher. This requires reliable predictions for the heat loads and the development of a mitigation strategy.

At ASDEX Upgrade, the diagnostics to investigate pedestal and plasma edge parameters as well as thermal loads to the first wall were significantly expanded and their time resolution improved during the past years. The Thomson scattering diagnostic was upgraded with a fast data acquisition system with a higher accuracy of the measured data and a much improved background treatment [4]. The available time resolution is now 2 µs in burst mode operation. The heat flux to the lower (main) divertor can be measured with a time resolution down to 65 µs routinely. In addition, a high spatial and temporal resolution 2D infra-red (ir) camera came into operation measuring the heat flux to the upper divertor and alternatively to non-divertor components, such as the central column, the ICRH and the protection limiters [5]. By changing the camera position, a nearly complete coverage of the inner surface is achieved. Radiative power losses from the plasma, the SOL, and the divertor are measured

by different bolometer systems. Recently, the bolometry evaluation algorithm was improved to get ELM resolved power balances [6]. Taking all diagnostics together, the all vessel heat load and (volume) radiation pattern can be measured with an ELM relevant time resolution. This paper will report on three selected topics of ITER relevance. (i) the heat load to non-divertor components in between and during ELMs, including ELM power balance, as well as the implication of fast particle and charge exchange loss for localised heat loads. (ii) ELM structures remote from the separatrix in the upper active divertor and at the limiters, and (iii) heat load to the inner wall during disruptions. The experimental arrangement of the ir-measurement outside the divertor is presented and discussed in [5]. Experimental details of the upper divertor measurements are presented in [7]. Further information on ASDEX Upgrade machine parameters and additional heating systems can be gained from [8, 9].

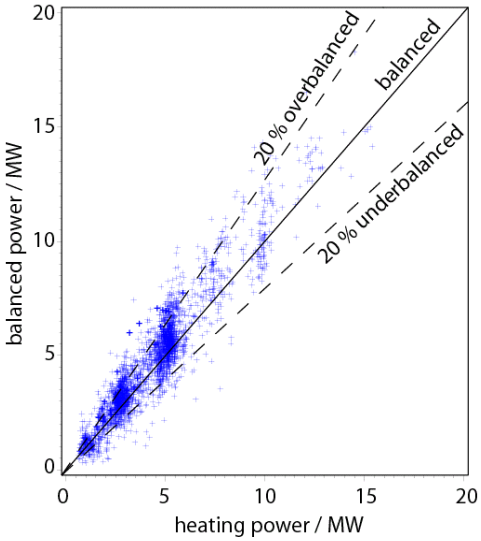

Fig. 1 Power balance in ASDEX Upgrade established from the heating power, the radiated power and the heat flux to the divertor. The data set comprises data from two experimental campaigns.

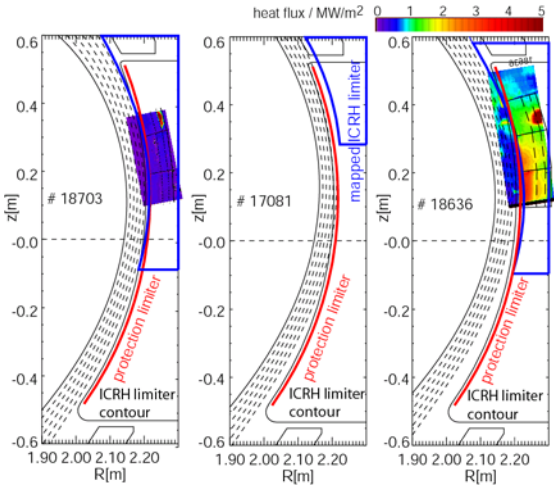

Fig. 2 Magnetic configurations together with limiter load as measured by the 2D ir-system. (Left) The protection limiter is shadowed. The hot spot is due to first orbit losses from a nearby neutral beam source (details see [10]). (Middle) The protection limiter is in front of the ICRH limiter. This configuration is used for the test limiter experiments. (Right) The upper part of the protection limiter is shadowed by the ICRH limiter and the deposited heat flux is reduced. The midplane distance between adjacent magnetic surfaces is 1 cm.

2. Heat load to non-divertor components

The power balance of ASDEX Upgrade established from heating power, power into the divertor and radiated power is equalized with an error of ± 20 % for a wide range of heating power, as shown in Fig. 1. Nevertheless, there are experimental results pointing on energy deposition to non-divertor components during different phases of a discharge. Thermographic investigation of ELM energy losses at ASDEX Upgrade and JET revealed that the energy detected in the divertor accounts for less than 100 % of the mid-plane losses [5, 10]. Besides the ELM heat deposition, visible and ir-diagnostics as well as energy deposition measurements by thermometry and calorimetry reveal that parts of the protection and ICRH antenna limiters are heated up to after-shot equilibration temperatures of 400 °C. Furthermore, hot spots are observed at different locations far away from the plasma in dependence on discharge configurations and conditions.

These non-divertor heat loads are caused by three mechanisms: (i) fast ions on ripple banana orbits penetrating into the limiter shadow, (ii) first orbit ion losses due to beam ionisation in

the limiter shadow or the plasma edge resulting in local overheating deep inside the divertor shadow, or (iii) charge exchange losses of fast ions in regions with high edge density, near the gas puff valves or in regions with locally enhanced recycling. The contribution of these mechanisms to the overall energy balance is small, but they contribute significantly to the production of impurities, which influence the plasma performance. A detailed discussion can be found in [10].

The heat penetration into the limiter shadow for inter-ELM as well as ELM phases is investigated by measuring the heat flux distribution at the protection limiters with the 2D ir-system. The four protection limiters in ASDEX Upgrade are geometrically 12 mm in the shadow of the ICRH antenna limiters (ICRHlim: R=2.20 m in the midplane). Nevertheless, they can receive a significant heat flux for specific plasma configurations.

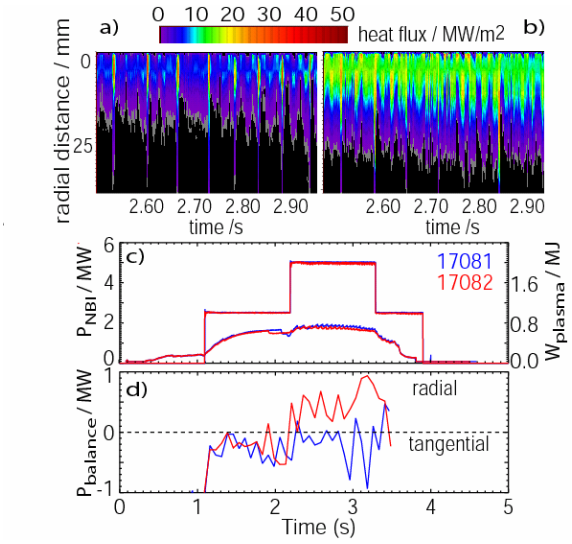

Fig. 3 Heat load to a test limiter for comparable discharges with tangential beam heating (a) and radial beam heating (b). Discharge parameters and power balance for the test limiter discharges are shown in the bottom (d) (I_p = 1 MA, B_t = -2T, q_{95} = 3.7).

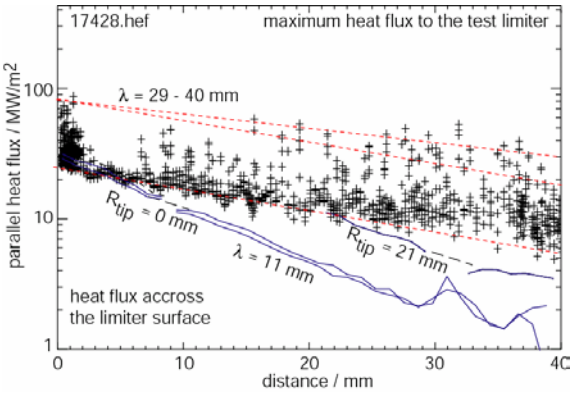

Fig. 4 Power e-folding lengths in the SOL and the limiter shadow as measured by moving the plasmas 4 cm away from the test limiter, starting at a gap distance of 2.5 cm in the midplane. The crosses are the maximum heat flux to the tip of the limiter. The base level of the tip heat flux corresponds to the inter ELM heat flux, the high levels to the ELM heat flux. The blue lines are the heat flux profiles measured across the (radial) surface of the test limiter for two different gap sizes. The discharge parameters are those of Fig. 3 (radial beams). Details of the experiment are published in [11].

For equilibrium configurations well adapted to the ICRH limiter shape (grey line in Fig. 2), the protection limiters are efficiently shadowed, but are at least partly accessible along field lines for plasma shapes deviating strongly from the ICRH limiter shape. In Fig. 2, the protection limiter is kept at the geometric coordinates and the ICRH limiter downstream (110 degrees in counter current direction), which is the active limiter for the ir-viewing geometry, is mapped along field lines onto the toroidal position of the protection limiter in view of the ir-camera. This partial shadowing is important for the interpretation of the limiter load measurements. The heat flux pattern shown in Fig. 2 reveals that limiters shadow the heat flux effectively for an appropriate magnetic configuration (Fig. 2 left). This holds also for ELMs. If the active limiter contour is a combination of ICRH and protection limiter, as shown in Fig. 2 right, the power e-folding length both in the far SOL and in the limiter shadow can be in principle derived.

The SOL heat flow and decay length in dependence on the neutral beam injection geometry is investigated by a test limiter exposed 5 mm in front of the ICRH limiter but magnetically about 40 mm out of the limiter shadow during two type-I ELMy H-mode shots with up to 5 MW heating power (see Fig. 3). The injection geometry was changed from tangential

beams located near to the test limiter to more radial beams toroidally 180 degrees away (for details of the NBI system see [9]). The averaged heat load to the tip of the limiter which is about half the parallel heat flux along field lines changes from about 5 MW/m^2 for the tangential beams to 12 MW/m^2 for the radial beams as shown in Fig. 3. Correspondingly the sum of radiation losses and power deposition to the lower divertor is reduced by about 500 kW or 10% of the heating power for the shot with higher test limiter load (see Fig. 3).

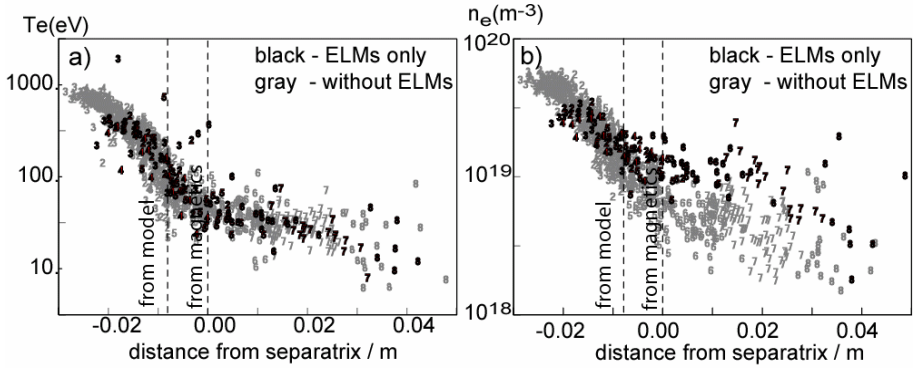

Fig. 5 ELM resolved temperature and density profiles as measured by Thomson scattering [4] show a steep gradient across the separatrix and a long tail remote from it. The separatrix position from the magnetic reconstruction is corrected by an energy transport model [12].

The reason for the measured difference in the heat load to the test limiter is the neutral beam injection geometry. While tangential beams create mostly well-confined passing particles, particles injected more radial in the plasma have a reduced parallel velocity component and as a consequence, a higher fraction is trapped on banana orbits at the low field side of the plasma. Particles on banana orbits with a width of a few cm can penetrate deep into the SOL and are scraped-off by the test limiter. A quantitative estimation of the fraction of banana transported power into the SOL needs kinetic code calculations, taking into account the magnetic field ripple and is in progress.

The ELM heat flux to the test limiter is about 50 MW/m^2 and nearly independent of the injection geometry (see Fig. 3), as expected from the MHD nature of the ELM instability.

The same test-limiter was used for heat flux decay measurements in the far SOL region by moving the plasma and changing the distance between the test limiter and the separatrix from 2.5 to 6.5 cm. The averaged heat load to the limiter tip is reduced with increasing distance to the separatrix resulting in an e-folding length of about 3-4 cm (Fig. 4) for the inter ELM phase (base line of the crosses) and the ELM heat load (top level of the crosses). The e-folding length in the test limiter shadow is nearly independent from the separatrix distance and with 11 mm (Fig. 4) shorter than the SOL decay length, as expected because of a shorter connection length. The similar decay lengths for ELM and inter ELM phases in the SOL and the limiter shadow means that the ratio of cross-field and parallel transport remains about constant. This is in qualitative agreement with the stiff ELM profile found at the outer divertor strike line [2].

The large e-folding length in a region far from the separatrix but in front of the limiters corresponds to the long tail of heat flux profiles as measured in the lower divertor which seems to be nearly constant over the observed distance of about 2 cm mapped to the midplane [5]. High resolution Thomson scattering measurements of plasma temperature and density in the edge also show a long tail in between and during ELMs [12, 13] remote from the separatrix as shown in Fig. 5.

A comparison of ELM energy losses in the midplane of ASDEX Upgrade and JET revealed that the energy detected in the divertor accounts for only about 50 % of the mid-plane losses. A significant fraction of the ELM energy should be deposited to non-divertor components or by a significantly increased radiation. The deposition to non-divertor components was investigated for a single discharge by a combination of fast local measurements at the limiter and the central column and thermometric energy measurement to get the toroidal distribution of the energy deposition [5]. For this discharge, about 25% of the ELM midplane loss was found at non-divertor components (see Table 1).

	ΔW_{mhd}	$W_{Antenna\ limiter}$	$W_{protection\ limiter}$	$W_{central\ column}$	$W_{outer\ divertor}$	$W_{inner\ divertor}$	*missing energy*
in kJ	*25*	*2.5*	*1.25*	*2.6*	*5*	*11*	*2.65*
in %	*100*	*10*	*5*	*10.4*	*20*	*44*	*10.6*

Table 1 Energy deposition per ELM to in-vessel components as measured with thermography. The data for the inner and outer divertor are averaged over 10 ELMs in the time range 2.0 to 2.2 s.

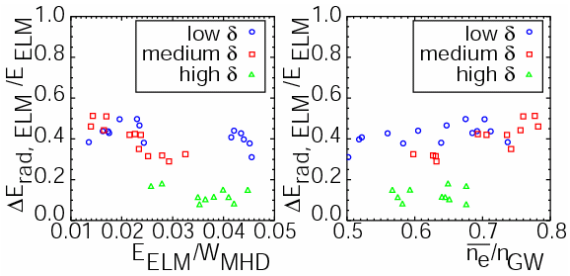

Fig. 6 Dependence of the normalized ELM radiation on the normalized ELM energy (left) and the normalised density (right) for discharges with 5MW heating power and q_{95} = 4.9.

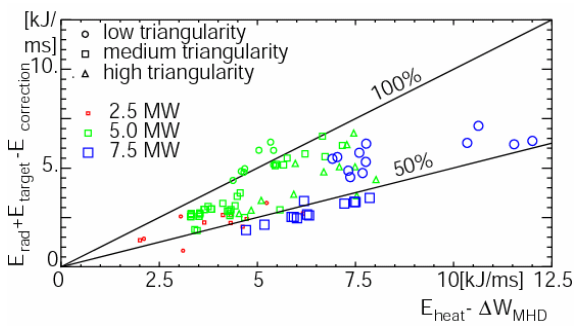

Fig. 7 Energy balance during ELMs balancing the input energy with the energy losses by radiation and the divertor heat load.

The improved calculation algorithm for the deconvolution of bolometer measurement allows to resolve ELMs on a time scale of 1 ms [6]. This is not sufficient to resolve the ELM itself, but allows to derive the ELM integrated radiated energy. This was done for a set of discharges with up to 7.5 MW heating power and magnetic configurations with low, medium and high triangularity. The fraction of radiated energy, $\Delta E_{rad}/E_{ELM}$ is between 40 % (low and medium triangularity) and 10 % (high triangularity) (see Fig. 6) with most of the energy radiated in the inner divertor. The ELM power balance established from the input power, the change of the plasma energy, the heat load to the divertor (corrected by the contribution of radiation in front of the divertor plates) and the radiated power is within 50 and 100 % (Fig. 7). Taking into account the non-divertor heat load due to ELMs of about 25 % [5], the power balance is slightly overbalanced. Radiation losses are a significant channel (20-40 % of the ELM midplane loss) for ELM energy dissipation in ASDEX Upgrade.

3. ELM structures remote from the separatrix

The power deposition during type-I ELMs as measured with a high resolution ir-system in the upper active divertor and at the outboard limiters show pronounced spatial structures on short time scales which will be discussed in the following.

In upper single null configurations, several, laterally displaced and inclined stripes, well separated from each other and from the main strike zone were found during type-I ELMs at the upper divertor plates remote from the separatrix (Fig. 8). These stripes were found in

addition to the toroidally symmetric heat deposition peak near to the separatrix, in particular in discharges with ion-grad-B drift direction away from the active x-point [7, 14]. They were interpreted as footprints of helical perturbations at the low field side of the main plasma edge related to non-linear ELM evolution. Based on this observation, the ELM related mode structure can be derived from the target heat load pattern, yielding on average toroidal mode numbers in a range of 8-24 [7, 14]. Despite the fact that the energy content of the sub-structures remote from the separatrix is less than 3 % [7] of the target load and no real concern for the divertor load in ITER, it allows insight into the temporal evolution of an ELM and the ELM mode structure.

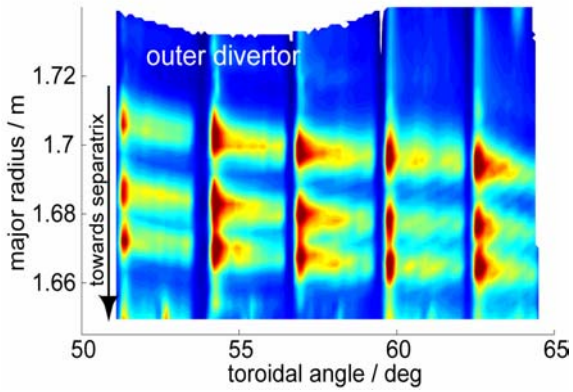

Fig. 8 Pronounced nonaxisymmetric deposition pattern during a type-I ELM measured in the upper outer divertor with the ion-grad B drift pointing away from the divertor.

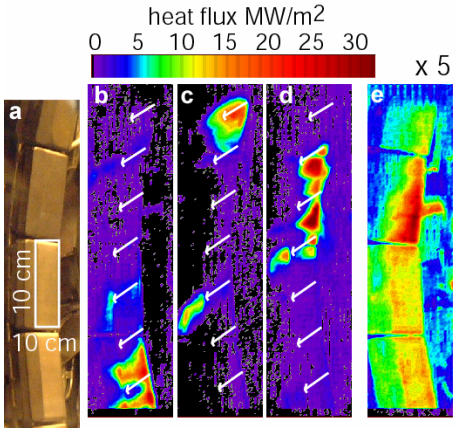

Fig. 9 ELM heat load pattern for single ELMs (b, c, d) at the protection limiter. The direction of the magnetic field is indicated by white arrows. The ELM averaged heat load (e) is below 5MW/m^2. The energy content of a single stripe is below 0.1% of the ELM midplane loss. (P_{NBI} = 5 MW, I_p = 1MA, B_t =-2T, q_{95} = 3.9). (a) Photograph view onto the limiter.

The heat flux deposited by single stripes varies by more than a factor of 5 with the tendency to be more equal with larger ELMs as discussed in [14]. This equal distribution of the power deposited into the stripes means that with increasing total ELM loss the ELM energy is split into more loss channels, i.e. a single stripe cannot remove all the ELM energy. The width of the stripes and the exposure parameters of the ir-camera allow to estimate the life time and a maximum rotation speed for the stripes [7]. The lifetime is longer than 120µs and clear evidence is found that strong stripes survive two consecutive frames or more than 250 µs at a fixed target position. The upper limit for rotation is estimated from the broadening of the stripes to about 300 Hz, about a factor of 10 lower than the time averaged toroidal rotation speed in the pedestal as measured with CXRS [7].

A localized heat deposition is also detected at the protection limiter. The heat flux pattern shows a strong spatial and temporal variation as shown in Fig. 9. The figure shows examples from one type-I ELMy H-mode discharge, but different ELMs. The height of a single limiter tile is 10 cm and corresponds to about 50 cm projected along field lines in ASDEX Upgrade for a safety factor, $q_{95,}$ of 4. There are clusters of stripes, but also well separated single stripes. The width of each stripe is 1 to 2 cm in poloidal direction with similar absolute values of the heat flux between 20 and 30 MW/m^2.

The uniform heat flux distribution in the cluster of four stripes shown in Fig. 9 d means that either the stripes are deposited simultaneously or their deposition time is much shorter than the 50 µs snapshot time of the measurement. Consecutive measurements with a frame

repetition rate of 500 µs show never a comparable structure and it should be concluded that the stripe deposition time is shorter than the frame repetition rate.

The energy content of a single stripe as estimated from the width, the measured heat flux and a deposition time of 50 µs is about 2 J, which has to be compared to 20 kJ plasma energy loss per ELM. Also the longest possible deposition time of 500 µs would result in energy deposition per stripe of only 0.1 % of the ELM energy loss. With typical toroidal mode numbers of 10 to 20 the stripe deposited ELM energy becomes 1-2 % of the ELM midplane loss. The main contribution of ELM energy deposition comes from a broader low level limiter heat flux following or in addition to the stripes as shown in the averaged ELM load with about 2-3 MW/m^2 over the whole limiter area. The inclination of the stripes follows essentially the helicity of the magnetic configuration as shown in Fig. 9 b,c,d and checked for discharges with different inclination of the magnetic field.

4. Inner wall load during disruptions

In ASDEX Upgrade most of the disruptions are caused by density limit, locked mode or by a loss of plasma control followed by a VDE [15, 16]. The energy release during the disruption is a two step process following a discharge phase where already a significant fraction (up to 89 %) of the thermal plasma energy is lost. Two main issues are investigated experimentally: the duration of the thermal quench and the foot print of the power deposition, i.e. the broadening of the SOL [17]. Both parameters strongly influence the extrapolation of thermal loads to ITER and finally the choice of the appropriate material [18]. The duration of the thermal quench as measured by thermography is in the order of a few milliseconds. The rising phase of the heat pulse on the strike point modules of the divertor lasts between 0.13 ms (time resolution of the measurements) and 1.5 ms. A fraction of the plasma thermal energy is deposited on the divertor during this phase of the pulse; a larger fraction reaches the divertor within the next 1-2 ms. If the duration of the thermal quench scales linearly with the minor radius of the experiment as predicted by theory, the ITER thermal quench time would be longer than the 1 ms assumed in the ITER design.

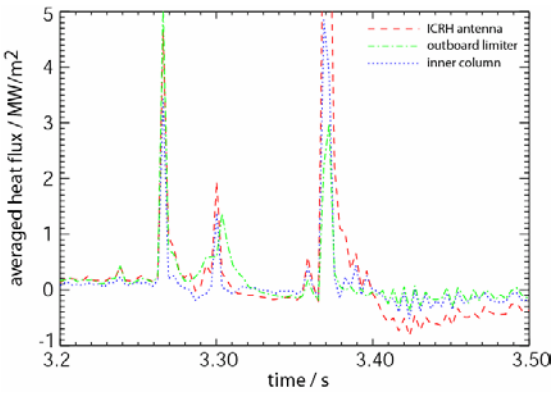

Fig. 10 Spatial averaged heat flux to different in-vessel components for a density limit discharge (18739) with 260 kJ plasma energy at 3 s.

The foot print of the power deposition during the thermal quench phase is significantly broadened compared to the heat flux deposition profile at the divertor target before the disruption. Power deposition profiles extend to the whole divertor [15, 17] and outside of it, as shown in Fig. 10 for a density limit disruption with 130 kJ energy loss in a minor disruption at 3.27 s and another 120 kJ in the thermal quench at 3.36 s.

The heat flux to non-divertor components, averaged over the duration of the thermal quench, is for this discharge about 2 MW/m^2 or about 100 kJ to the inner vessel surface of 50 m^2. This broadening of the power deposition during the thermal quench is significant higher than the factor 3 assumed for ITER.

5. Summary

The power deposition to non-divertor components was investigated with high temporal resolution. The mechanisms causing local heat loads to non-divertor components, partly deep in the limiter shadow, are qualitatively understood. The long tail of the heat flux profile measured in the outer divertor is extended to the outer SOL with an e-folding length of a few centimetres in between and during ELMs, respectively. The power decay length measured in the limiter shadow is shorter (about 1 cm). The ELM resolved power balance reveals that up to 40 % of the ELM midplane loss is radiated away and 25 % are deposited non-radiative to non-divertor components. Stripe-like heat deposition in the active upper divertor and at the limiter was measured during ELMs. The contribution of a single stripe to the ELM energy balance is small (below 1 %). The phenomenology of the stripes can be explained by toroidally localized sources in the outer midplane with a certain radial extend, mapped along field lines to the divertor and limiters. The heat load pattern during the thermal quench phase of disruptions shows a broad distribution, covering not only the whole divertor, but also non-divertor components. The duration of the power deposition is in the order of 1 ms.

6. References

[1] LACKNER, K., "private communication"; 2004.
[2] HERRMANN, A., et al., "Stationary and transient divertor heat flux profiles and extrapolation to ITER", J. Nucl. Mater. 313-316*:*759; 2003.
[3] FUNDAMENSKI, W., et al., "Narrow power profiles seen at JET and their relation to ion orbit losses", J. Nucl. Mater. 313*:*787-795; 2003.
[4] KURZAN, B., et al., "Signal processing of Thomson scattering data in a noisy environment in ASDEX Upgrade", Plasma Phys. Contr. Fus. 46*:*299-317; 2004.
[5] HERRMANN, A., et al., "Power deposition outside the divertor in ASDEX Upgrade", Plasma Phys. Contr. Fus. 46*:*971-979; 2004.
[6] FUCHS, J. C., et al., "Radiation distribution and energy balance during type-I ELMs in ASDEX Upgade", J. Nucl. Mater. PSI 2004, Portland; 2004.
[7] EICH, T., et al., "Type-I ELM substructure on the divertor target plates in ASDEX Upgrade", Plasma Phys. Control. Fusion accepted for publication; 2004.
[8] HERRMANN, A., et al., "Chapter 1: ASDEX upgrade introduction and overview", Fusion Science and Technology 44*:*569-577; 2003.
[9] STREIBL, B., et al., "Chapter 2: Machine design, fueling, and heating in ASDEX upgrade", Fusion Science and Technology 44*:*578-592; 2003.
[10] HERRMANN, A., et al., "Interaction of ELMs and fast particles with in-vessel components in ASDEX Upgrade", J. Nucl. Mater. PSI 2004, Portland; 2004.
[11] YE, M. Y., et al., "Tungsten Limiter Tests in ASDEX Upgrade", Journal of Nuclear Materials. submitted; 2004.
[12] NEUHAUSER, J., et al., "Transport into and across the Scrape-off Layer in the ASDEX Upgrade Divertor Tokamak", Plasma Phys. Control. Fusion 44*:*855-870; 2002.
[13] NEUHAUSER, J., et al., "Chapter 8: Edge and divertor physics in ASDEX Upgrade", Fusion Science and Technology 44*:*659-681; 2003.
[14] EICH, T., et al., "Nonaxisymmetric energy deposition pattern on ASDEX upgrade divertor target plates during type-I edge-localized modes", Phys. Rev. Lett. 91; 2003.
[15] PAUTASSO, G., et al., "Analysis of the power deposition in the ASDEX Upgrade divertor during disruptions", Europhysics Conference Abstracts (CD-ROM, Proc. of the 30th EPS Conference on Controlled Fusion and Plasma Physics, St. Petersburg 2003).
[16] PAUTASSO, G., et al., "Chapter 12: Study of disruptions in ASDEX upgrade", Fusion Science and Technology 44*:*716-729; 2003.
[17] PAUTASSO, G., et al., "Details of power depostition in the thermal quench of ASDEX Upgrade disruptions", Europhysics Conference Abstracts (CD-ROM, Proc. of the 31th EPS Conference on Controlled Fusion and Plasma Physics, London 2004).
[18] LOARTE, A., et al., "Expected energy fluxes onto ITER plasma facing components during disruption thermal quenches from multi-machine data comparisons", IAEA 2004 (this conference); 2004.